Illusory contours using shape information*

Wei Zhu† and Tony Chan‡

February 12, 2003

Abstract

Recognizing illusory contour figures in images is an intrinsic capability of human vision. Many models have been proposed to single out the illusory contours figures. In this paper, we choose a different point of view to understand the phenomena about illusory contours, i.e., we would like to find the best matching between illusory figures which is determined by illusory contours, and known shapes, which means our model doesn't concentrate only on the information of visual cues, such as L-junctions, T-junctions, in images. We consider here two cases, the first one is to find the illusory figures with exact known shape, while the second case permits an affine transformation of known shape, which allows a much larger classes of illusory figures to be found. Finally, at the end of this paper, we present results for many synthetic illusory figures including classical ones, such as Kanizsa triangle and square.

1. Introduction

Illusory contour figure is a very common and well-known phenomena in human vision. These figures are not composed of concrete objects, but induced by some parts of boundaries of interest in images, and these boundaries are insufficient to consist of a closed boundary. Moreover, these figures lie among the objects in images, and always have the same gray level as background. Therefore, among all illusory contour figures, a common character is that part of the boundaries are missing. However, based on the information of existing boundaries, human being can always recognize the hidden shapes, i.e, can complete all the missing boundaries. Classical examples are the Kanizsa triangle and square which are shown in Figure 1. For these two images, human visual system may fill in the missing parts for the hidden triangle and square, then induce sharp perceptual contours, even though they are not present.

*This work has been supported partly by ONR contract N00014-96-1-0277, NSF contract DMS-9973341 and NIH contract P20 MH65166

†Department of Mathematics, Univeristy of California, Los Angeles, 405 Hilgard Avenue, Los Angeles, CA 90095-1555. E-mail: wzhu@math.ucla.edu.

‡Department of Mathematics, Univeristy of California, Los Angeles, 405 Hilgard Avenue, Los Angeles, CA 90095-1555. E-mail: TonyC@college.ucla.edu.

Figure 1. Kaniza triangle, square and a special illusory triangle. Human being may easily identify a triangle and a square in the first two graphs respectively, even though parts of their boundaries are missing, which means that human visual can fill in the missing parts to get complete figures. However, in the third graph, without the shape information of triangle, the illusory triangle may not be recognizable.

To understand this phenomena, many models have been proposed. The models can be divided into two kinds, with one kind involving completing the boundary of special interests using the information of corners and boundaries, such as Geiger [3], Ullman [4], etc., while the other kind employing the whole regions, Sarti [10] etc. Regardless of the kind, the methods all exploit the information of the existing boundary or corners as much as possible. For example, in Geiger's paper [3], first, they pick out all the corners in the image, such as T-junctions, L-junctions, etc, then they set out a set of hypothesis for each corner, as there are several possible explanations for each corner; next, by minimizing some "energy", they can select the best set of hypothesis (image organization), then get the illusory figures. Taking a different way, Sarti, Mallidi and Sethian[10] begin with an initial surface, which is chosen on the basis of a reference point inside the illusory contour figures, then flow the surface according to the image gradient, the flow will sharpen the surface around the existing edges and complete the missing edges.

In this paper, we take a totally different perspective to understand illusory contour figures in images. Our idea is this: we first assume the shape of the illusory figure is known, then we search in the equivalent class of the shape for the suitable object which matches the illusory contour the best. For example, to identify Kaniza triangle in Figure 1, we take the shape of equilateral triangle, and choose a figure with this shape to match the image, such that it just overlaps the Kaniza triangle perfectly, which means Kaniza triangle is determined. For Kaniza square, we will take the shape of an equilateral square. In this way, by taking the shape of equilateral triangle, we may single out the illusory triangle for the third image in Figure 1, even though many proposed methods are not applicable for this case. Basically, in this paper, we consider only one shape. But in general, we expect the methodology can be extended to a library of shapes.

The difference between our method and others lies primarily in several ways: First, our model employs known shapes as candidates to segment the image to find the illusory figures, which means we initially assume the illusory contour figures have some known shapes or an affine transformation of some known shapes. Hence, our model doesn't distinguish the illusory contour figures with straight line boundaries or the ones with any curves as boundaries, which is different from Sarti's method[10], where they prefer to fill in the missing parts with straight lines. Second, not as other models, our model doesn't concentrate only on visual cues such as T-junctions, L-junctions, etc, that is, we need not to analyze the possible cases for each corner, such as Geiger's [3]. In addition, since our model is area-wise not point-wise, small perturbation of the shape could be allowed. Third, our model requires no strict initial guess position for the goal illusory figures, which means a reference point, such as in Sarti [10], or something else of the illusory figures is unnecessary.

The paper is organized as follows. Section 2 consists of several parts. In section 2.1, a review for shapes representation using signed distance functions [8] will be given. In section 2.2, we will discuss two cases about searching for illusory figures, that is, one is to search for illusory figures in the equivalent class of known shape, which means the shape of illusory figures is exact the known shape, while the second case is to single out the illusory figures in the collection of shapes which are affine transformations of known shapes. The two models to each case will be proposed in section 2.3 and section 2.4 respectively. In section 3, two groups of experiments will be presented according to each case, including classical example such as Kanizsa triangle, square and some artificial examples, and followed by a comparison of searching for different illusory figures with identical initial searching figures by the second model. A conclusion will be given in section 5.

2. Models

2.1 A review of shapes representation using signed distance functions

As discussed in Paragios, Rousson and Ramesh's work [8], we would like to use a particular level set function–signed distance functions–to represent a shape. Explicitly, given an object Ω in R^2, according to its boundary, there exists a signed distance function which is positive inside Ω and negative outside Ω, that is, a viscosity solution can be found for the following equation:

$$\begin{array}{c} \mid \nabla\phi \mid = 1 \\ \phi \begin{cases} > 0 & x \in \Omega \setminus \partial\Omega \\ = 0 & x \in \partial\Omega \\ < 0 & x \in R^2 \setminus \Omega \end{cases} \end{array} \tag{1}$$

where Ω is assumed to be a closed bounded set in R^2.

In this way, any object in the plane corresponds a unique signed distance function, and vice versa. Instead of seeing shapes of objects as isolated ones, we may regard a shape as an equivalent relation in the collection of objects, since it is invariant to translation, scaling and rotation. Any two objects in the same equivalent class will have an identical shape. Moreover, all the signed distance functions for the objects in an equivalent class should have the same form, only differ in some parameters. For example, let object Ω be a representative from an equivalent class of shape, and ϕ be the corresponding signed distance function, then consider another object Ω_1, which is a translation $(a, b) \in R^2$ of Ω, then the signed distance function to Ω_1 will be $\phi_1(x, y) = \phi(x - a, y - b)$. Similarly, we may get the signed distance functions for the objects by scaling or rotating Ω. That is, if $\widehat{\Omega}$ belongs to the equivalent class of which Ω is a representative, then its corresponding signed distance function is just a composition of the signed distance functions given by the three operations–translation, scaling and rotation. Explicitly, let $\widehat{\phi}$ be the corresponding signed distance function of $\widehat{\Omega}$, then there exists a four-tuple (a, b, θ, r), such that

$$\widehat{\phi}(x, y) = r\phi\left[\frac{(x-a)\cos\theta + (y-b)\sin\theta}{r}, \frac{-(x-a)\sin\theta + (y-b)\cos\theta}{r}\right], \quad (2)$$

where (a, b) represents the center of rotation, θ the angle for rotation, r the scaling factor. It is easy to check that $\mid \nabla\widehat{\phi} \mid = 1$.

We can see there is a bijective mapping T from Ω to $\widehat{\Omega}$ as follows: $T(\begin{bmatrix} x \\ y \end{bmatrix}) = \frac{1}{r}\begin{bmatrix} \cos\theta & \sin\theta \\ -\sin\theta & \cos\theta \end{bmatrix}\begin{bmatrix} x-a \\ y-b \end{bmatrix}$ for any $(x, y) \in \Omega$. That is to say, $\widehat{\phi} = r\phi \circ T$. Moreover, the orthogonal matrix $\begin{bmatrix} \cos\theta & \sin\theta \\ -\sin\theta & \cos\theta \end{bmatrix}$ is the key thing to keep the shape. If we choose a general matrix $\begin{bmatrix} a_{11} & a_{12} \\ a_{21} & a_{22} \end{bmatrix}$ for the mapping T, the shape would be changed unless the matrix is an orthogonal one.

2.2 A Discussion of searching for illusory figures with exact and perturbed known shape

In this paper, we would like to consider two cases of searching for illusory figures. The first one is to search in images for illusory figures whose shapes are exactly the same as known ones, while the second one deals with the ones whose shapes are affine transformations of known shapes. Hence, in the process of searching for the illusory figures, the objective figures will keep the same shape for the first case, while can be changeable for the second case, but restricted to the collection of shapes which are affine transformation of the known shapes.

It seems that the two cases differ in the transformations between known shapes and those of illusory figures. Actually, they can be categorized in a common frame— a linear transformation. For the first case, the transformation we choose, $\begin{bmatrix} \cos\theta & \sin\theta \\ -\sin\theta & \cos\theta \end{bmatrix}$ for a suitable angle θ, belongs to $O(2)$, if we

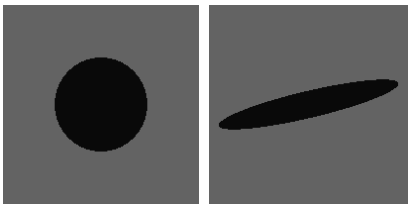

Figure 2. The graph on the left is a circle, while the right one is an ellipse which is a transformation from the circle by matrix $A = \begin{bmatrix} 5 & 1 \\ 1 & 1 \end{bmatrix}$. The comparison shows that a general transformation in $GL(2,2)$ may change the shape considerably.

omit the scaling factor r, since we keep the shape in the process of searching. While for the second case, the transformation could be chosen in a large space of matrix, that is $GL(2,2)$, in which the matrix takes the form $\begin{bmatrix} a_{11} & a_{12} \\ a_{21} & a_{22} \end{bmatrix}$, with $\det \begin{bmatrix} a_{11} & a_{12} \\ a_{21} & a_{22} \end{bmatrix} \neq 0$, $a_{ij} \in R^1$, $i,j = 1,2$. Moreover, we require that the matrix chosen in $GL(2,2)$ be close to $\begin{bmatrix} \cos\theta & \sin\theta \\ -\sin\theta & \cos\theta \end{bmatrix}$ for some θ in some sense, since we prefer the shapes of illusory figures look close to the known shapes. For example, if we choose the matrix $A = \begin{bmatrix} 5 & 1 \\ 1 & 1 \end{bmatrix}$, the shapes should be horrible shown in Figure 2. Hence, we may look the shapes of the illusory figures as a perturbation of known shapes.

In the next two sections, we will discuss the models for the above two cases.

2.3 The model for exact shapes.

In this paper, to explain our model clearly, we assume that the images of interest have the following property: there are two parts, i.e, *objects* and *background*, inside the images; they take positive values for the *objects* and negative values for the *background*. For example, for Kaniza triangle in Figue 1, we may set positive values for the three black parts (*objects*) and negative values for the rest (*background*). In the following context, we will always use the the terms "*objects*" and "*background*" for this kind of images.

Many segmentation models could be used to get this kind of images. For example, Chan and Vese's model [1] could separate objects from background easily, yielding a level set function with positive values on the objects and negative values for the background.

Now, let u be an image of interest on domain R, and suppose u takes positive value on the *objects* inside the domain R, while negative value for the *background*. In our model, instead of taking u directly, we will consider $B(u)$

which is defined as:

$$B(u) = \begin{cases} 1 & if\ u > 0 \\ 0 & if\ u \leq 0 \end{cases} . \tag{3}$$

Actually, $B(\cdot)$ is just the Heaviside function. Since u will not be updated in our model, we prefer to denote it as $B(u)$. Therefore, we just consider images in which *objects* and *background* are separable.

In addition, we assume the illusory figure takes a known shape. For example, in Kanizsa triangle in Figure 1, we know the shape of the illusory figure is an equilateral triangle.

To single out the illusory figure in an image, we will try to match it with a figure in the equivalent class of the known shape. We will call the figure as *objective* figure later on. For example, for Kanizsa triangle in Figure 1, we may take an objective figure with the shape of equilateral triangle to match the image, and by updating the four-tuple (a, b, θ, r) of the objective figure, which is mentioned in section 2.1, we can get the best matching—the objective figure just overlaps Kanizsa triangle perfectly, which means we find the illusory figure.

Naturally, according to the properties of illusory figures, there are two requirements to describe the best matching.

1). The objective figure should lie among all the *objects* in the image, since we consider here the illusory figure is an "inside" one, i.e., it is always surrounded by *objects* in images. In Kanizsa triangle in Figure 1, the illusory triangle is surrounded by the three objects.

2). The objective figure should overlap the *objects* in the image as less as possible. Also in Kaniza triangle in Figure 1, the goal objective figure should only touch the three objects.

We will take advantage of shapes representation using signed distance functions mentioned in Section 2.1 to construct an energy satisfying the two requirements. Employing the distance is the key thing of our model.

Let u be an image with the property mentioned at the beginning of this section, φ_0 be the signed distance function of a figure with the known shape, which is assumed to be the shape of the illusory figure, and φ be the signed distance functions of *objective* figures, which has the same form as φ_0, only differs in the values of the four-tuple (a, b, θ, r).

For the first requirement, we recall that φ is the signed distance function corresponding to the objective figure characterized by $\varphi \geq 0$, that is, $\mid \varphi(p) \mid$ measures the distance from point p to the boundary $\varphi = 0$. As the objective figure should lie among all the *objects* in the image, or the *objects* should distribute around the objective figure as close as possible, which equivalently says the sum of all the distances from each point of the *objects* to the boundary $(\varphi = 0)$ of the objective figure should be as small as possible. We may choose an intergral to discribe this sum as follows:

Figure 3. In these two graphs, the white curves represent the boundaries ($\varphi = 0$) of the two different objective figures. The amount $\int_R B(u)\varphi^2 dxdy$ for the right one is smaller than that of the left one, which means that the objective figure for the right case lies "closer" to the *objects* than the left one does, or closer to the desirable Kanizsa triangle in some sense.

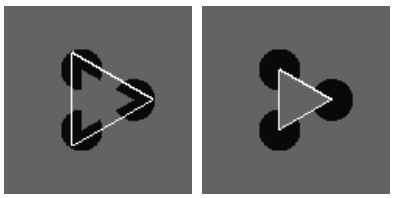

Figure 4. In these two graphs, the white curves represent the boundaries ($\varphi = 0$) of the two different objective figures. The amount $\int_R B(u)\varphi^2 dxdy$ for the left case is smaller than that of the right case, but a correct illusory figure is obtained in the right graph. This comparison validates that only $\int_R B(u)\varphi^2 dxdy$ is insufficient to single out the illusory figure in an image of interest.

$$\int_R B(u)\varphi^2 dxdy. \tag{4}$$

Here, we incorporate the term $B(u)$ in the integral because we only need the sum of all the distance from any points of the *objects* in the image, while the region $\{(x,y) \in R:\ B(u(x,y)) = 1\} = \{(x,y) \in R:\ u(x,y) > 0\}$ represents the union of the *objects*.

An illustration in Figure 3 shows that different objective figures will induce different values of (4). As the amount becomes smaller, the objective figure will be closer to the *objects*.

However, this term is insufficient to single out the illusory figure. This could be illustrated by Figure 4, where the amount $\int_R B(u)\varphi^2 dxdy$ shown in the left case is smaller than that of the right case, but the right case yields the desirable illusory figure.

This could be solved by introducing another term, which just satisfies the second requirement. The new term reads

$$\int_R B(u)H(\varphi)\varphi^2 dxdy. \tag{5}$$

Figure 5. In this graph, the white curve represents the boundary ($\varphi = 0$) of the objective figure. The objective figure is trapped into a local minimizer of (6), i.e., it will not converge to the desirable illusory triangle. This example shows the energy (6) is also insufficient to find out the illusory figure if a good initial guess of the objective figure is not given.

Here $H(\cdot)$ is the Heaviside function. As

$$\{p \in R:\ B(u(p))H(\varphi(p)) = 1\} = \{p \in R:\ u(p) > 0\} \cap \{p \in R:\ \varphi(p) > 0\},$$

the term $\int_R B(u)H(\varphi)\varphi^2 dxdy$ just represents the sum of the distances from all the overlapping points between the *objects* and the objective figure to the boundary of objective figure ($\varphi = 0$). This term will prevent large overlapping.

We combine the two terms (4) and (5) in this way:

$$\int_R B(u)\varphi^2 dxdy + \lambda \int_R B(u)H(\varphi)\varphi^2 dxdy, \tag{6}$$

where λ be a parameter which controls how much the overlapping can be allowed.

Basically, this model is appliable for finding illusory figures with a good initial guess of the objective figure, because it will always be trapped into a local minimizer, which is illustrated by Figure 5.

To this end, we need to add one more term, which controls the scaling factor of the objective figure, that is, r, which is mentioned in Section 2.1. This term reads

$$r^2 L^2 \int_R B(u)H(\varphi)dxdy, \tag{7}$$

where L balances the dimension difference between the value φ and r. This term states if there is an overlap between the objective figure and the *objects* in the image, i.e., $\int_R B(u)H(\varphi)dxdy > 0$, the scaling factor r of the objective figure should be decreased.

Hence, we have the energy:

$$E(\varphi) = E(a, b, r, \theta) =$$

$$\int_R B(u)\varphi^2 dxdy + \lambda \int_R B(u)H(\varphi)\varphi^2 dxdy + \mu r^2 L^2 \int_R B(u)H(\varphi)dxdy, \tag{8}$$

where λ and μ are two parameters.

To simplify our model, we prefer to revise our energy by combining the last two terms, and then it reads

$$E(\varphi) = E(a, b, r, \theta) = \int_R B(u)\varphi^2 dxdy + \lambda \int_R B(u)H(\varphi)(\varphi + rL)^2 dxdy, \quad (9)$$

where λ is a parameter controling the overlapping, L is a scaling constant compensating for the dimension difference between φ and r, and

$$\varphi(x, y) = r\varphi_0 \left[\frac{(x-a)cos\theta + (y-b)sin\theta}{r}, \frac{-(x-a)sin\theta + (y-b)cos\theta}{r} \right], \quad (10)$$

or we can write as $\varphi(x, y) = r\varphi_0 \circ T(x, y)$, where

$$T(\begin{bmatrix} x \\ y \end{bmatrix}) = \frac{1}{r} \begin{bmatrix} \cos\theta & \sin\theta \\ -\sin\theta & \cos\theta \end{bmatrix} \begin{bmatrix} x-a \\ y-b \end{bmatrix}, \quad (11)$$

$H(\cdot)$ is the Heaviside function, i.e.,

$$H(x) = \begin{cases} 1 & x > 0 \\ 0 & x \leq 0 \end{cases} . \quad (12)$$

The energy (9) involves the four-tuple (a, b, θ, r) which are the parameters for different objective figures in the same shape equivalent class mentioned in section 2.1. To minimize the energy is to update the four parameters, which is different from many other conventional models which take functions as updating ones.

In summary, our model contains two parts. The first one $\int_R B(u)\varphi^2 dxdy$ describes the position of the objective figure ($\varphi > 0$) according to the *objects* in the image. As the objective figure lies among the *objects*, $\int_R B(u)\varphi^2 dxdy$ will be small. The second term $\lambda \int_R B(u)H(\varphi)(\varphi+rL)^2 dxdy$ represents the overlapping between the objective figure and the *objects* in the image. Parameter λ will control how much the overlapping can be permitted.

Remark It is readily seen that the value of the parameter λ will affect the final result, and as λ becomes big enough, the final result will be the desirable illusory figure. This fact could be demonstrated Figure 6.

As mentioned in the introduction, our model differs from other models in several ways. First, our model involves four parameters describing shapes, not a function. Second, in our model, we take a known shape, that is, we suppose the hidden illusory figure takes the shape, then search for the illusory figure in the given image. Hence, our model doesn't distinguish the illusory contour figures with straight line boundaries or the ones with any curves as boundaries, which is different from Sarti's method[10], where they prefer to fill in the missing parts

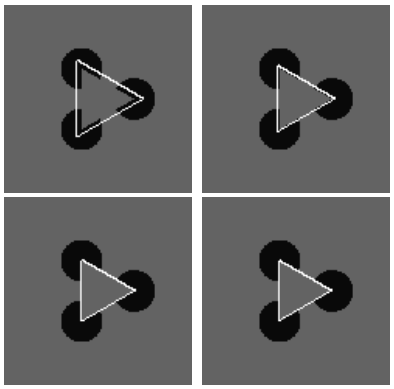

Figure 6. In this group of graphs, the white curves represent the boundaries ($\varphi = 0$) of the final objective figures corresponding to the four cases with $\lambda =$ 0.1, 0.5, 1.0, 2.0 (The order is from left to right, from the first row to the second row). These graphs demonstrate that as λ is big enough (here $\lambda \geq 1.0$), the final objective figure will be the same one, i.e., the desirable illusory figure.

with straight lines. Third, not as other models, our model doesn't concentrate only on visual cues such as T-junctions, L-junctions, etc, that is, we need not to analyze the possible cases for each corner, such as Geiger's [3]. In addition, since our model is area-wise not point-wise, small perturbation of the shape could be allowed. Fourth, there is no requirement of the initial objective figure, which is different from Sarti [10] in which a reference has to be chosen.

To minimize the above energy (6), we may update the four parameters a, b, r, θ by the conventional gradient decent method.

We may assume that a, b, r, θ are all functions of time t, that is, the process of decreasing the energy is equivalent to time evolving. Then the energy $E(a, b, r, \theta)$ becomes an function of t. Therefore,

$$\frac{dE}{dt} = \int_R \Big[B(u) 2\varphi \frac{d\varphi}{dt} + \lambda B(u)\delta(\varphi)(\varphi + rL)^2 \frac{d\varphi}{dt}$$

$$+\lambda B(u) H(\varphi) 2(\varphi + rL)\left(\frac{d\varphi}{dt} + L\frac{dr}{dt}\right)\Big] dxdy$$

$$= \int_R B(u) \left[2\varphi + \lambda\delta(\varphi)(\varphi + rL)^2 + \lambda H(\varphi) 2(\varphi + rL)\right] \frac{d\varphi}{dt} dxdy$$

$$+ \int_R \left[\lambda B(u) H(\varphi) 2(\varphi + rL) L\right] \frac{dr}{dt} dxdy. \tag{13}$$

For simplicity, we denote

$$A = B(u)(2\varphi + \lambda\delta(\varphi)(\varphi + rL)^2 + \lambda H(\varphi)2(\varphi + rL)). \tag{14}$$

Then

$$\frac{dE}{dt} = \int_R A\frac{d\varphi}{dt}dxdy + \int_R \lambda B(u)H(\varphi)2(\varphi + rL)L(\frac{dr}{dt})dxdy. \tag{15}$$

As

$$\frac{d\varphi}{dt} = \left[-\varphi_0 + \varphi_{0x}\frac{(x-a)\cos\theta + (y-b)\sin\theta}{r} + \varphi_{0y}\frac{-(x-a)\sin\theta + (y-b)\cos\theta}{r}\right]$$

$$(-\frac{dr}{dt}) + (\varphi_{0x}\cos\theta - \varphi_{0y}\sin\theta)(-\frac{da}{dt}) + (\varphi_{0x}\sin\theta + \varphi_{0y}\cos\theta)(-\frac{db}{dt})$$

$$+ [\varphi_{0x}((x-a)\sin\theta - (y-b)\cos\theta) + \varphi_{0y}((x-a)\cos\theta + (y-b)\sin\theta]\,(-\frac{d\theta}{dt}), \tag{16}$$

where $\varphi_{0x} = \frac{\partial\varphi_0}{\partial x}$, $\varphi_{0y} = \frac{\partial\varphi_0}{\partial y}$.

Therefore, if we choose

$$\frac{da}{dt} = \int_R A(\varphi_{0x}\cos\theta - \varphi_{0y}\sin\theta)dxdy, \tag{17}$$

$$\frac{db}{dt} = \int_R A(\varphi_{0x}\sin\theta + \varphi_{0y}\cos\theta)dxdy, \tag{18}$$

$$\frac{dr}{dt} = \int_R A\left[-\varphi_0 + \varphi_{0x}\frac{(x-a)\cos\theta + (y-b)\sin\theta}{r}\right.$$

$$\left.+\varphi_{0y}\frac{-(x-a)\sin\theta + (y-b)\cos\theta}{r}\right]dxdy - \int_R \lambda B(u)H(\varphi)2(\varphi + rL)Ldxdy, \tag{19}$$

$$\frac{d\theta}{dt} = \int_R A\left\{\varphi_{0x}\left[(x-a)\sin\theta - (y-b)\cos\theta\right]\right.$$

$$\left.+\,\varphi_{0y}\left[(x-a)\cos\theta + (y-b)\sin\theta\right]\right\}dxdy, \tag{20}$$

then $\frac{dE}{dt} \leq 0$, which means the energy will decrease if we update a, b, r, θ in the direction of (17), (18), (19) and (20) respectively.

2.4 The model for perturbed shapes.

As discussed in the last section, our model takes advantage of some known shape information to find out the illusory figures in images. For many cases, the illusory figures may not be the exact same shapes as known shapes, but close to the later ones in some sense. For instance, an equilateral triangle and an unequilateral one. We can regard these shapes as "perturbations" of the known shapes. Hence, in the searching for illusory figures, instead of the transformation only in $O(2)$, an affine transformation in $GL(2,2)$ should be allowed. However, this doesn't mean that we could choose any matrix in $GL(2,2)$, instead we should take some control for this matrix, in fact, a loose control could lead to undesirable shapes which don't converge to what we need. To this end, we would like to add a new term involving the matrix in $GL(2,2)$ to the energy discussed in the last section.

The new term involves how to take control of the matrix $\begin{bmatrix} a_{11} & a_{12} \\ a_{21} & a_{22} \end{bmatrix}$. In this paper, we control the matrix in this way, that is, we hope the chosen matrices are close to some orthogonal ones, $\begin{bmatrix} \cos\theta & \sin\theta \\ -\sin\theta & \cos\theta \end{bmatrix}$ for some θ. In fact, let $A \in GL(2,2)$, if AA^T is close to I in the norm $\| \cdot \|_2$, then A is close some orthogonal matrix $\begin{bmatrix} \cos\theta & \sin\theta \\ -\sin\theta & \cos\theta \end{bmatrix}$. Where $\| A \|_2 = \sqrt{\sum_{i,j=1}^{2} a_{ij}^2}$, $A = (a_{ij})$, I is the identity matrix, and A^T means the transpose of A. This fact implies that $\| AA^T - I \|_2^2$ should be small. On the other hand, as the shapes of our goal illusory figures could be transformations of known shapes, $\| AA^T - I \|_2^2$ should not be required to be 0, which only yield the same shape as known ones. Hence, a threshold ε is needed. As $\| AA^T - I \|_2^2 > \varepsilon$, that is, the shape is far from given shape, the amount $\| AA^T - I \|_2^2$ should be decreased; while $\| AA^T - I \|_2^2 \leq \varepsilon$, it should be free of updating for the entries in A.

In summary, we have the revised energy as:

$$E(\varphi, A) = E(a, b, r, a_{11}, a_{12}, a_{21}, a_{22}) =$$

$$\int_R B(u)\varphi^2 dxdy + \lambda \int_R B(u)H(\varphi)(\varphi + rL)^2 dxdy$$

$$+\mu H(\| AA^T - I \|_2^2 - \varepsilon), \tag{21}$$

where λ and μ are parameters, with λ controlling the overlapping between the objective figure and the *objects* in the image, and μ controlling how much the perturbation of the shape can be allowed; L is a scaling constant compensating for the unit difference between φ and r; ε is the threshold describing what kind of shapes are permitted; $H(\cdot)$ is the Heaviside function, and

$$A = \begin{bmatrix} a_{11} & a_{12} \\ a_{21} & a_{22} \end{bmatrix},$$

the function φ takes the form as:

$$\varphi(x,y) = r\varphi_0\left[\frac{a_{11}(x-a)+a_{12}(y-b)}{r}, \frac{a_{21}(x-a)+a_{22}(y-b)}{r}\right], \qquad (22)$$

or we can write as $\varphi(x,y) = r\varphi_0 \circ T(x,y)$, where

$$T(\begin{bmatrix} x \\ y \end{bmatrix}) = \frac{1}{r}\begin{bmatrix} a_{11} & a_{12} \\ a_{21} & a_{22} \end{bmatrix}\begin{bmatrix} x-a \\ y-b \end{bmatrix} = \frac{1}{r}A\begin{bmatrix} x-a \\ y-b \end{bmatrix}. \qquad (23)$$

In this revised model, the new arguments are $a, b, r, a_{11}, a_{12}, a_{21}, a_{22}$, where a, b, r are the same as what discussed in the last section, and the matrix A represents an affine transformation in $GL(2,2)$, not the orthogonal one $\begin{bmatrix} \cos\theta & \sin\theta \\ -\sin\theta & \cos\theta \end{bmatrix}$.

Actually, in this new model, φ is not a signed distance function any more, but it is close to a signed distance function in some sense. In fact, $\mid \nabla\varphi \mid^2 = \begin{bmatrix} \varphi_x & \varphi_y \end{bmatrix}\begin{bmatrix} \varphi_x & \varphi_y \end{bmatrix}^T = \begin{bmatrix} \varphi_{0x} & \varphi_{0y} \end{bmatrix} AA^T \begin{bmatrix} \varphi_{0x} & \varphi_{0y} \end{bmatrix}$, where $\varphi_x = \frac{\partial\varphi}{\partial x}$, $\varphi_y = \frac{\partial\varphi}{\partial y}$, it means that if $\parallel AA^T - I \parallel_2^2$ is very small, $\mid \nabla\varphi \mid^2 \simeq \begin{bmatrix} \varphi_{0x} & \varphi_{0y} \end{bmatrix}\begin{bmatrix} \varphi_{0x} & \varphi_{0y} \end{bmatrix}^T = \mid \nabla\varphi_0 \mid^2 = 1$.

Similarly, we may derive as last section the formulas for updating the arguments $a, b, r, a_{11}, a_{12}, a_{21}, a_{22}$.

3. Experiments

In this section, first, we would like to present two groups of results, one for the first case in section 3.1, including classical illusory figures such as Kanizsa triangle and square, the other for the second case in section 3.2, including general triangle, parallelogram and ellipse, whose shapes are transformations of equilateral triangle, square and circle respectively. Finally, in section 3.3, by applying the second model, a comparison of searching for different illusory figures by the second model with an identical initial objective figure will be given.

Each of the results consists of a process of searching for the illusory figures, that is, starting from the initial objective figure, and ending at the convergent objective figure. The order is from top row to bottom row, and from left to right, i.e, the top left figure is the initial one. The initial objective figures can be chosen freely, that is, no particular requirement about their position, scale, and angle is needed, which is important, since we have no information where the illusory figures are in many cases. Additionally, in each graph, to make it easy to distinguish the objective figure from the image, we take a white curve to represent it in the way that the white curve is just the boundary of the objective figure.

All the images are defined on the domain $[-4,4] \times [-4,4]$, the mesh $\Delta x = \Delta y = h = \frac{8}{N}$, where $N = 120$, and $L = 1$. Different parameters and time step size dt are chosen accordingly for each experiment.

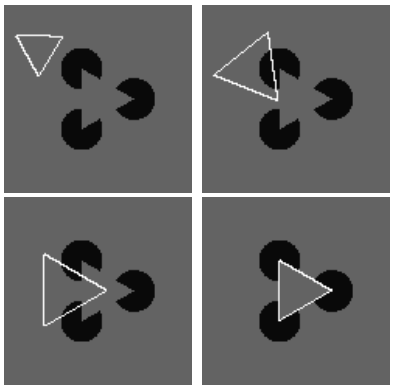

Figure 7.1. Searching for Kanizsa triangle (equilateral triangle) in the equivalent shape class of equilateral triangle. In the sequence, the objective figure approaches the Kanizsa triangle while translating, scaling and rotating simultaneously. In this experiment, time step size $dt = 0.01$, $\lambda = 2.0$.

3.1 Experiments for exact shape

The first two examples are the classical illusory figures–Kanizsa triangle and square (Figure 7.1 and Figure 7.2). We present the process of searching for them, that is, we search for the figure which matches the Kanizsa triangle or square in the equivalent shape class of equilateral triangle or square respectively.

The third illusory figure is also an equilateral triangle, but the triangle is rotated a little compared with Kanizsa triangle (Figure 7.3). The example shows that our model is also capable for general situation for illusory figures, not only for classical illusory figures.

The fourth example is also an illusory equilateral triangle (Figure 7.4). In this example, the corners of triangle are not shown as any visual cues such as L-junctions or T-junctions. Any method that uses L-junctions or T-junctions may not be applicable for this case. However, as our model takes the shape as an global objective, we still can identify the illusory triangle. In another word, without the shape of triangle, the illusory triangle here is difficult to be recognized.

The illusory figures are disks (circles) in the next two examples (Figure 7.5 and Figure 7.6). We present here two cases about disks, one is a classical illusory figure, with a disk in a square, another is a disk in an equilateral triangle. We would like to show that our model can handle shapes with curves as the boundary, not merely the straight lines such as triangles in the former examples. Because our model takes the shape globally as an objective, and any shape could be considered, regardless of its straight or curved boundary. In addition, in these two examples, only three of the four-tuple (a, b, θ, r), that is, a, b, r will be updated, since a rotation is not needed for a disk, which is implied by the model itself.

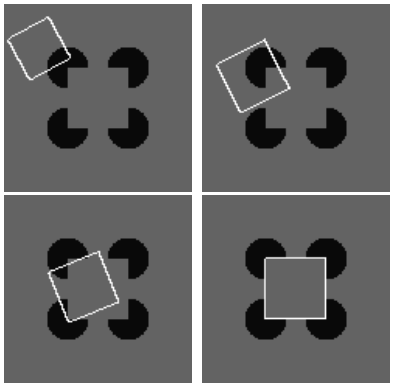

Figure 7.2. Searching for Kanizsa square in the equivalent shape class of square. In the sequence, the objective figure approaches the Kanizsa square while translating, scaling and rotating simultaneously. In this experiment, time step size $dt = 0.01$, $\lambda = 2.0$.

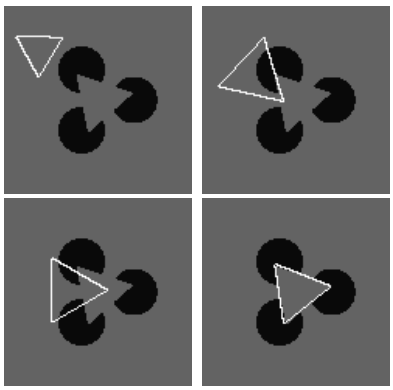

Figure 7.3. Searching in the image for an illusory equilateral triangle in the equivalent shape class of equilateral triangle. This image is different from Kanizsa triangle in that the illusory triangle is rotated a little compared with Kanizsa's. The example shows that our model is capable for some general situation for illusory figures, not only for classical ones. In this experiment, time step size $dt = 0.01$, $\lambda = 2.0$.

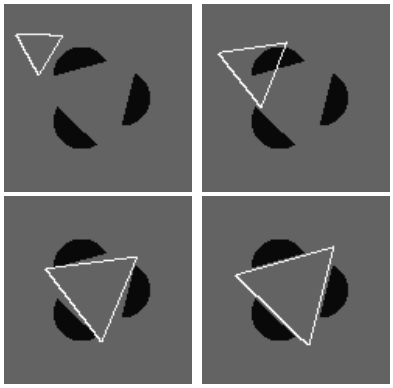

Figure 7.4. Searching in the image for an illusory equilateral triangle in the equivalent shape class of equilateral triangle. In this example, the corners of triangle are not shown as any visual cues such as L-junctions or T-junctions. Any method that uses L-junctions or T-junctions may not be applicable for this case. This example shows the importance of the shape to recognize illusory figures. In this experiment, time step size $dt = 0.02$, $\lambda = 1.5$.

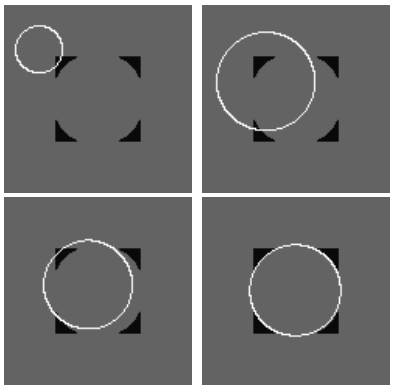

Figure 7.5. Searching in the image for an illusory disk in the equivalent shape class of disks. In this example, the illusory figure has curved boundary, not straight lines. This example shows our model is capable of finding illusory figures with curved boundaries. In this experiment, time step size $dt = 0.05$, $\lambda = 0.2$.

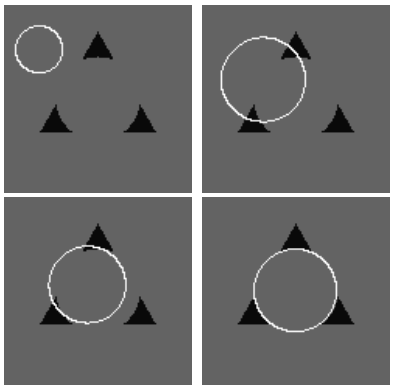

Figure 7.6. Searching in the image for an illusory disk in the equivalent shape class of disks. In this example, the illusory figure has curved boundary, not straight lines. This example shows our model is capable of finding illusory figures with curved boundaries. In this experiment, time step size $dt = 0.05$, $\lambda = 0.5$.

The last example is an illusory equilateral triangle immersed in a group of black bars (Figure 7.7). The example is different not only from Kanizsa triangle but also from the fourth example discussed above. First, the corners of the illusory triangle are not presented as L-junction or T-junction. Second, the illusory triangle touches the black bars not by its continuous edges but by several discrete parts of its edges. This example implies that our model is also capable of singling out illusory figures from some "messy" environment.

3.2 Experiments for perturbed shape

In this section, we would like to show some experiments for the second case in section 3.2, that is, searching for the illusory figures, whose shapes are not exactly identical to known shapes, but affine transforms of known shapes. This allows a larger class of illusory figures to be found with limited known shapes. In the following experiments, the known shapes are equilateral triangle, square and circle (disk), and the illusory figures we try to find are general triangles, parallelograms and ellipses respectively.

The first experiment is to search for the an illusory triangle (not an equilateral triangle), starting from an initial equilateral triangle, in the class of shapes which are transformation of an equilateral triangle (Figure 8.1).

The second experiment is to search for the an illusory parallelograms (not a square), starting from an initial square, in the class of shapes which are transformation of equilateral square, that is, parallelograms (Figure 8.2).

The third experiment is to search for an illusory ellipse, which is a transformation of a circle, starting from a circle, in the class of shapes which are transformation of a circle, that is, ellipses (Figure 8.3).

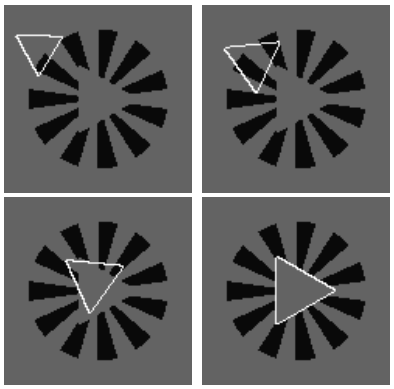

Figure 7.7. Searching in the image for an illusory equilateral triangle in the equivalent shape class of equilateral triangle. In this example, the corners of the illusory triangle are not presented as L-junction or T-junction, and it touches the black bars not by its continuous edges but by several discrete parts of its edges. The example validates that our model is also capable of singling out illusory figures from some "messy" environment. In this experiment, time step size $dt = 0.002$, $\lambda = 6.0$.

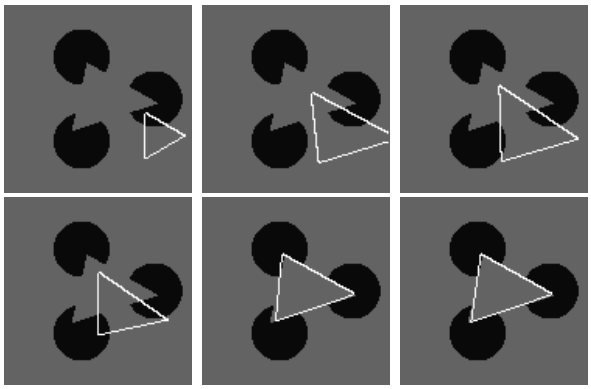

Figure 8.1. Searching in the image for the triangle (not an equilateral triangle) in the class of shapes which are transformations of the shape of an equilateral triangle. The initial objective figure is an equilateral triangle. In the sequence of graphs, the shapes keep evolving from time to time, and as the shapes are far from an equilateral triangle, they will evolve back close to the latter one. This is different form the situation in Figure 7.1 where the shape keeps invariant. In this experiment, time step size $dt = 0.01$, $\lambda = 1.5$, $\mu = 100.0$, $\varepsilon = 0.2$.

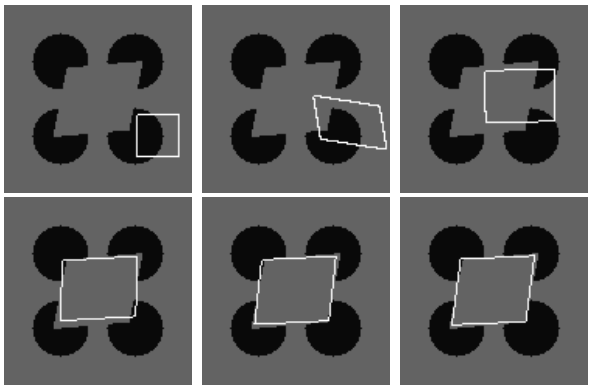

Figure 8.2. Searching in the image for the parallelograms (not a square) in the class of shapes which are transformations of a square. The initial objective figure is a square. In the sequence graphs, the shapes keep evolving from time to time, and as the shapes are far from a square, they will evolve back close to a square. This is different form the situation in Figure 7.2 where the shape keeps invariant. In this experiment, time step size $dt = 0.0075$, $\lambda = 2.0$, $\mu = 100.0$, $\varepsilon = 0.2$.

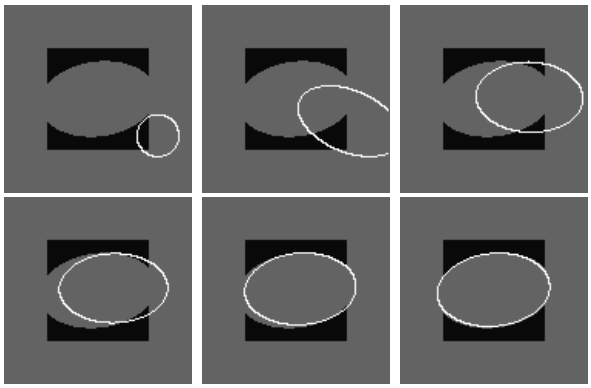

Figure 8.3. Searching in the image for the ellipse (not a circle) in the class of shapes which are transformations of a circle. The initial objective figure is a circle. In the sequence graphs, the shapes keep evolving from time to time, and as the shapes are far from a circle, that is, as the ellipse are too stretched, they will evolve back close to a circle. This is different form the situation in Figure 7.5 where the shape keeps invariant. In this experiment, time step size $dt = 0.01$, $\lambda = 0.5$, $\mu = 100.0$, $\varepsilon = 0.4$.

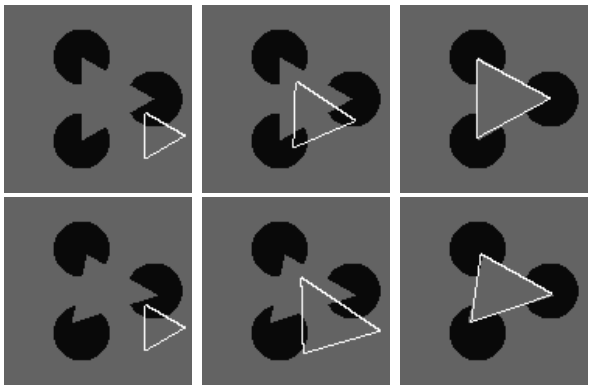

Figure 9.1. The top row is the searching process (initial, intermediate and final step, from left to right) for Kanizsa triangle. With the same initial searching figure, another searching process for a general triangle (not an equilateral triangle) is shown in the bottom row. They are both done with the second model. This comparison validates that the second model in section 2.4 can be applied for finding some general triangles with the shape of an equilateral triangle.

3.3 A comparison of searching for different illusory figures by an identical initial objective figure with the second model

In this section, by applying the second model, a comparison of searching for different illusory figures with an identical initial objective figure will be presented by several experiments. This validates that the second model in section 2.4 allows a larger shape class of illusory figures than the first model in section 2.3 with a known shape, and the first model is just a special case of the second one.

For each group of graphs (Figure 9.1 and Figure 9.2), the top row represents a searching process (initial, intermediate and final step) for an illusory figure, while for another illusory figure in the bottom row. But, they start from an identical initial objective figure.

4. Conclusion

In this paper, we employ the idea of matching to find out illusory figures in images with known shape information, which is completely different from many other methods, such as Geiger's [3], Sarti's [10] and so on. We consider two cases, one is to search for illusory figures in the equivalent class of known shape, which means the known shape is exact the shape of illusory figures, while the second case is to single out the illusory figures in the class of shapes which are affine transformation of known shapes, which makes our method applicable for a

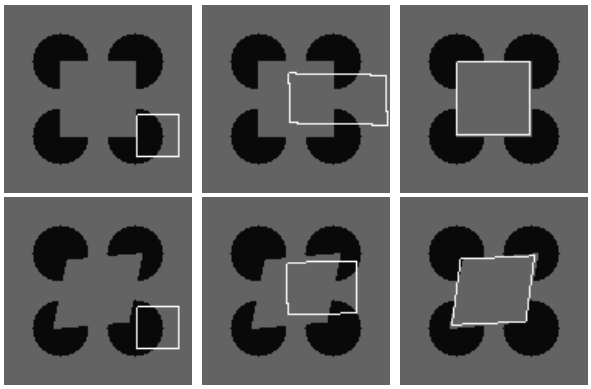

Figure 9.2. The top row is the searching process (initial, intermediate and final step, from left to right) for Kanizsa square. With the same initial searching figure, another searching process for a general parallelogram (not a square) is shown in the bottom row. They are both done with the second model. This comparison validates that the second model in section 2.4 can be applied for finding some general parallelograms with the shape of a square.

broad of illusory figures. The experiments listed in section validate our models.

5. Acknowledgments

The first author would like to thank Dr. Selim Esedoglu for telling us Geiger's work.

6. References

[1] T. Chan and L.A. Vese, Active contours without edges. *IEEE Transaction on Image Processing*, 10(2): 266-277, February 2001.

[2] D. Geiger, K. Kumaran and L. Parida, Visual Organization for Figure/Ground Separation.

[3] D. Geiger, H.K. Pao and N. Rubin, Salient and Multiple illusory surfaces. In IEEE Computer Society Conference on Computer Vision and Pattern Recognition, June 1998, Santa Barbara, CA.

[4] S.Ullman. Filling in the gaps: The shape of subjective contours and a model for their generation. Biological Cybernetics, 25:1-6, 1976.

[5] S. Osher and J. A. Sethian, Fronts Propagating with Curvature-Dependent Speed - Algorithms Based on Hamilton-Jacobi Formulations, *J. Comput. Phys*, *Vol* 79, $12 - 49$, 1988.

[6] H.K. Pao and D. Geiger, A continuous Shape Descriptor by Orientation Diffusion. In the 3rd International Workshop, EMMCVPR, Sep. 2001, France, pp. 544-559.

[7] H.K. Pao, D. Geiger and N. Rubin, Measuring Convexity for Figure/Ground Separation. In 7th International Conference on Computer Vision, Sep. 1999, Kerkyra, Greece.

[8] N. Paragios, M. Rousson and V. Ramesh, Matching Distance Functions: A Shape-to-Area Variational Approach for Global-to-Local Registration. Copenhangen, Denmark, 2002.

[9] M.Rousson and N. Paragios, Shape Priors for Level Set Representations.

[10] A. Sarti, R. Malladi and J.A. Sethian, Subjective surfaces: A method for completing missing boundaries. Proceedings of the National Academ of Sciences of the United States of America, Vol 12, N.97, pag. 6258-6263,2000.

[11] H.K. Zhao, T. Chan, B. Merriman and S. Osher, A variational level set approach to multiphase motion.$J.Comput.Phys.$, $127 : 179 - 195, 1996$.